

# Physicochemical characterization of residual potato (*Solanum tuberosum*) starch recovered from the potato chips industry in Mexico

Caracterización fisicoquímica de almidón recuperado de papa (*Solanum tuberosum*) residual de la industria de papas fritas en México

Montoya-Anaya Diana G.<sup>1</sup>, Madera-Santana Tomas J.<sup>2</sup>, Aguirre-Mancilla Cesar L.<sup>1</sup>, Grijalva-Verdugo Claudia<sup>1</sup>, Gonzales-Garcia Gerardo<sup>3</sup>, Nuñez-Colín Carlos A.<sup>3</sup>, Rodriguez-Nuñez Jesus R.<sup>4,\*</sup>.

<sup>1</sup> Postgraduate Department, National Technological of Mexico/I. T. Roque, km 8 Carretera Celaya-Juventino Rosas, Celaya, Guanajuato, 38110, México.

<sup>2</sup> Food and Development Research Center, A.C. CTAOV, A.P. 1735, Hermosillo, Sonora, 83304, Mexico.

<sup>3</sup> Department of Chemistry, DCNyE, University of Guanajuato, Noria Alta s/n. Guanajuato, Gto. 36050, Mexico.

<sup>4</sup> Biotechnology Program, University of Guanajuato. Mutualismo #303, Colonia La Suiza, Celaya, Guanajuato, 38060, Mexico.

## ABSTRACT

The objective of this study was to evaluate the physicochemical, morphological, structural, and thermal properties of starch recovered from *Solanum tuberosum* residual of chips industry in Mexico using advanced instrumental techniques. The residual potato was collected from a chips production company and the starch obtained by aqueous extraction. The starch presented a content of carbohydrates of 87.79 %, proteins (1.18 %), lipids (0.15 %), ashes (0.26 %), and amylose (24.35 %). The water absorption capacity was 1.0163 g g<sup>-1</sup>, solubility (30.17 - 46.65 %), swelling (2.31 - 8.69 g g<sup>-1</sup>). Thermal analyzes showed a starch gelatinization about 61.7 - 90 °C with a maximum weight loss at 288.1 °C. The scanning electron microscopy-energy dispersive spectroscopy (SEM-EDS) showed particles of 14 - 69 μm with a composition of 54.3 % carbon, 45.4 % oxygen, and 0.15 % potassium. The dynamic light scattering (DLS) showed particles of nanometric size (120 nm). The nuclear magnetic resonance (NMR) and X-Ray diffraction (XRD) exhibited the crystallinity of the starch as type B (34.73 %) and the Fourier transform infrared spectroscopy-attenuated total reflectance (FTIR-ATR) showed the functional groups distinctive of the glucose.

**Keywords:** amylose, crystallinity, functional properties, instrumental characterization, agroindustrial byproduct.

## RESUMEN

El objetivo de este estudio fue evaluar las propiedades fisicoquímicas, morfológicas, estructurales y térmicas del almidón recuperado de los residuos de *Solanum tuberosum* de la industria de frituras en México, utilizando técnicas instrumentales avanzadas. La papa residual se recogió de una empresa productora de papas fritas y el almidón se obtuvo mediante extracción acuosa. El almidón presentó un contenido de carbohidratos de 87.79 %, proteínas (1.18 %), lípidos (0.15 %), cenizas (0.26 %) y amilosa (24.35 %). La capacidad de absorción de agua fue de 1.0163 g g<sup>-1</sup>, solubilidad (30.17 - 46.65 %), hinchamiento (2.31 - 8.69 g g<sup>-1</sup>). Los análisis térmicos mostraron una gelatinización del almidón entre 61.7 - 90 °C con una pérdida máxima de peso a 288.1

°C. La microscopía electrónica de barrido-espectroscopía dispersiva de energía (SEM-EDS) mostró partículas de 14 - 69 μm con una composición de 54.3 % de carbono, 45.4 % de oxígeno y 0.15 % de potasio. La dispersión dinámica de luz (DLS) mostró partículas de tamaño nanométrico (120 nm). La resonancia magnética nuclear (NMR) y la difracción de rayos X (XRD) exhibieron la cristalinidad del almidón como tipo B (34.73 %) y la reflectancia total atenuada por espectroscopía infrarroja transformada de Fourier (FTIR - ATR) mostró los grupos funcionales distintivos de la glucosa.

**Palabras clave:** amilosa, cristalinidad, propiedades funcionales, caracterización instrumental, subproducto agroindustrial.

## INTRODUCTION

The potato (*Solanum tuberosum*) is one of the most economically and socially important foods, currently as the third most consumed crop worldwide, only surpassed by wheat, and rice (Devaux *et al.*, 2021). In 2019, world potato production was 370 million tons, of which Mexico produced more than 1 million, presenting a per capita consumption of 14.8 kg (FAOSTAT, 2020; Devaux *et al.*, 2021). It is estimated that around 56 % of the national production is used for fresh consumption, processing companies demand 29 %, while 15 % is destined for seed (Mejía and Castellanos, 2018).

In the industrialization of this tuber, approximately 88.9 % of the product is used, the remaining percentage corresponds to the residues generated (Calvache *et al.*, 2022). For the processing of potatoes, both external (size, shape, presence of diseases, defects, deformations, cold and mechanical damages) and internal (total solids, non-reducing and total sugars, flavor, and nutritional value) characteristics are considered to ensure the quality of the final product, those that do not meet the requirements are rejected and considered waste (Ortega and Andrade-Bolaños, 2021).

About 25 % of the waste generated during potato processing is disposed of in sanitary landfills, in unsuitable places or deposited in agricultural plots for degradation, without going through a process that gives them an add

value (Sánchez-Castelblanco and Heredia-Martín, 2021; Calvache *et al.*, 2022). The concern for the use of residues has gained great strength worldwide, in the scientific community and especially at the industrial level, where production processes generate by-products that can be useful in other activities (Quintero *et al.*, 2015), such as use of starch in the case of potato, since, in addition to its importance as a food, it has expansive uses in the industry mainly due to its starch content (Jagadeesan *et al.*, 2020).

Starch is a polysaccharide composed of glucose monomers that form the amylose (20 - 30 %) and amylopectin, the amylose is formed by 1,4- $\alpha$ -D-glucose monomers with a linear structure and small number of long branches, meanwhile, the amylopectin is formed by 1,6- $\alpha$ -D-glucose monomers with a high-density branched chain, these branching occurs every 20 to 23 glucose units (González-Cuello *et al.*, 2016; Kowsik and Mazumder, 2018). The amylose-amylopectin ratio varies significantly between starches depending on their source, such as the type and variety of plant or fruit, as well as growth conditions. Several studies have shown that this variation involves changes in their physicochemical characteristics and interactions with other molecules, resulting in different functional and microscopic properties, as well as different texture and stability of starch products (Lemos *et al.*, 2019). Then, it is possible to recover and make an advanced characterization of the residual potato starch used in the manufacture of potato chips in Mexico.

Potato starch is preferred over others, because its paste has high clarity and neutral flavor (Alvani *et al.*, 2011), attributed to the high content of phosphate esters in the amylopectin chain (Šimková *et al.*, 2013). In 2015, the starches annual world production was approximately 85 million tons (Dupuis and Liu, 2019), with corn, wheat, potato, and rice starch being the main sources, accounting for 84 %, 7 %, 4 % and 1 %, respectively (Basiak *et al.*, 2017). This starch is widely used in industrial sectors, such as food, feed, paper, textiles, laundry finishes, chemical, petrochemical, pharmaceutical industries, bioethanol, construction materials and biodegradable products (Maniglia *et al.*, 2020). In this sense, the objective of this study was to evaluate the physicochemical, morphological, structural, and thermal properties of starch recovered from potato (*Solanum tuberosum*) residual of chips industry in Mexico, using advanced instrumental techniques, to offer alternatives for the recycling of residual potatoes.

## MATERIALS AND METHODS

### Starch extraction

The residual potato was collected from a chips production company, located in the industrial zone in the state of Mexico, Mexico. It was then washed, the skin removed, and their size was reduced using a homemade grater. The grated potatoes were soaked for 30 min with constant manual agitation (100 g of potato/200 mL of water), then filtered using a domestic sieve; this process was repeated three times (50 mL of water/100 g of potato). The filtrate was left undisturbed for 1 hour and the starch recovered by decantation and subjected

to two washes using distilled water. Finally, the recovered starch was dried at 60 °C and stored in hermetically sealed plastic bags until use (Vargas *et al.*, 2016).

### Proximate composition analysis

Moisture content was determined using a thermobalance (OHAUS™ MB35) according to Pardo *et al.* (2013), total ash content was determined using the dry ash method (Kirk *et al.*, 1991), and protein content was determined by the Kjeldahl method (factor of 6.25), according to the Official Mexican Standard NOM -F-68-S -1980. Additionally, the Soxhlet method was used to determine the total lipid content (James, 1999) and total carbohydrates were estimated as the percentage remaining to reach 100 % of the proximal composition (Valle *et al.*, 2019).

Amylose content was determined using the methodology of Hoover and Ratnayake (2001). Specifically, defatted starch (25 mg) was dissolved in 10 mL of 90 % dimethylsulfoxide (DMSO), stirred for 20 min, and then maintained for 15 min in a water bath at 85 °C. The mixture was cooled and gauged with 25 mL of distilled water. An aliquot (1 mL) was taken and diluted with 5 mL of iodine solution (0.0025 mol L<sup>-1</sup>) in potassium iodide (0.0065 mol L<sup>-1</sup>) (I<sub>2</sub>/KI) and gauged to 50 mL with distilled water. The absorbance was read at 600 nm using a spectrophotometer (Multiskan™ GO, Thermo Scientific™, USA), mixtures of DMSO and iodine solution in potassium iodide were used as blank. The amylose content of the starch sample was determined using a standard curve prepared from potato amylose and amylopectin mixtures (Sigma Aldrich, Edo. de México), containing 0 - 100, 10 - 90, 20 - 80, 30 - 70, 40 - 60, 50 - 50, 60 - 40, 70 - 30, 80 - 20, 90 - 10 and 100 - 0 % treated in the same way as starch solutions. All determinations were analyzed in triplicates.

### Functional properties

#### Water absorption capacity

To determine the starch water absorption capacity, suspensions of 5 % starch in 40 mL of distilled water were prepared, left to stand for 40 min with stirring every 10 min, and centrifuged (Thermo Scientific™ Sorvall™ ST 8 Centrifuge) at 3250 rpm for 25 min at 25 °C. The supernatant was discarded, and the sediment was weighed to determine the adsorption capacity (eq.1). The test was performed in triplicate (Sindhu *et al.*, 2019).

$$\% \text{ WAC} = \frac{\text{sediment weight (g)} - \text{initial sample weight (g)}}{\text{initial sample weight (g)}} \quad \text{eq.(1)}$$

#### Solubility and swelling power

The determination of the solubility index (SI) and swelling power (SP) was determined by the method of Meaño *et al.* (2014) with some modifications. Specifically, 1 % starch suspensions were prepared in 40 mL of distilled water, heated in a water bath (Ecoline Staredit. LAUDA® E100) at 60 °C, 70 °C, 80 °C and 90 °C for 30 min, then cooled to 25 °C, and centrifuged (Thermo Scientific™ Sorvall™ ST 8 Centrifuge) at 4000 rpm for 50 min.

The supernatant was discarded, while the gel formed was recovered and dried at 60 °C for 20 hours to determine the SI (eq.2) and the SP (eq.3).

$$SI(\%) = \frac{\text{dry gel weight (g)}}{\text{initial sample weight (g)}} \times 100 \dots\dots \quad \text{eq.(2)}$$

$$SP(g/g) = \frac{\text{wet gel weight (g)}}{\text{initial sample weight (g)} - \text{dry gel weight (g)}} \quad \text{eq.(3)}$$

### Morphological and optical analysis

#### Scanning electron microscopy (SEM) and elemental analysis (EDS)

Morphological analysis of the starch surface was performed at 100X and 200X using a scanning electron microscope (JEOL, JSM-7600 F, Japan). Starch particles were coated with a thin layer of Au-Pd using a sputter coater (Quorum Q150R-ES, Sussex, UK) before scanning. The morphological analysis of starch particles was performed to investigate size and shape. In addition, the elemental composition of samples was analyzed using an Oxford X-Max 20 energy dispersive X-ray spectroscopy (EDS) detector and an Oxford wavelength dispersive X-ray spectroscopy (WDS) detector (Acosta-Ferreira *et al.*, 2020).

#### Dynamic Light Scattering (DLS)

Particle size, polydispersity index (PDI) and zeta potential of starch were determined using a DLS instrument, Zetasizer Nano ZS (Malvern Instruments Ltd., Worcestershire, UK), according to the method reported by Sattari *et al.* (2017), with some modifications. Specifically, 1.2 mg of the sample was dissolved in 2 mL of 95 % EtOH, subsequently sonicated for 5 min in an ultrasound bath to disintegrate the starch granules, and then placed in a polystyrene cuvette for reading in the equipment. All results were recorded as the average of 5 measurements.

#### Color

Starch color was determined using a Chroma Meter colorimeter (Minolta CR-400 Japan) calibrated with a white mosaic standard ( $Y = 94.1$ ;  $X = 0.3155$ ;  $Z = 0.3319$ ). Color was read using the CIE Lab scale and measured (L) luminosity (0 black to 100 white) and chromaticity parameters  $a^*$  (- 100 green to + 100 red) and  $b^*$  (- 100 blue to + 100 yellow). Five replicates of the sample were analyzed, placed on the pattern. The color difference ( $\Delta E$ ) was calculated using equation 4.

$$\Delta E = \sqrt{(\Delta L^*)^2 + (\Delta a^*)^2 + (\Delta b^*)^2} \quad \text{eq.(4)}$$

Where  $\Delta L^* = L^* - L_0$ ,  $\Delta a^* = a^* - a_0$  and  $\Delta b^* = b^* - b_0$ .  $L_0$ ,  $a_0$  and  $b_0$  represent the color parameters of the standard, while  $L^*$ ,  $a^*$  and  $b^*$  represent the color parameters of the sample (Gonçalves *et al.*, 2020).

### Thermal analysis

#### Differential Scanning Calorimetry (DSC)

Starch gelatinization properties were analyzed using a Differential Scanning Calorimeter (DSC) on a Discovery model from TA Instruments Inc. (New Castle, DE). Specifically, 10 mg of sample were placed in aluminum cells and sealed under pressure. An empty aluminum cell was used as a reference. Both cells were heated from 20 to 180 °C at a heating rate of 10 °C/min and then rapidly cooled to 20 °C. The thermal parameters determined of the gelatinization peak were, initial temperature ( $T_0$ ), maximum temperature ( $T_p$ ), final temperature ( $T_f$ ) and gelatinization enthalpy ( $\Delta H$ ), typical of the starch gelatinization process (Rodríguez-Núñez *et al.*, 2014).

#### Thermogravimetric analysis (TGA/DTGA)

Thermal decomposition of starch was analyzed using a TA Instruments Discovery Model Thermogravimetric Analyzer (TGA) (New Castle, DE). A sample of approximately 20 mg was heated from 50 to 600 °C at a heating rate of 10 °C/min, under an inert  $N_2$  atmosphere with a flow rate of 60 mL/min (Rodríguez-Núñez *et al.*, 2014).

### Structural analysis

#### NMR spectra

$^{13}C$  nuclear magnetic resonance analyzes were performed on a Bruker Avance III spectrometer (USA, Massachusetts) operating at 500 MHz using  $CDCl_3$ . NMR spectra were referenced using the residual signal of  $CHCl_3$  at 77.26 ppm (chemical shifts) (Gómez and González-García, 2018).

#### X-ray diffraction (XRD)

To determine the crystalline structure of starch, a powder sample was placed in a sample holder for X-ray diffractometry. The X-ray diffraction patterns were obtained using a Bruker D8-Advance Bragg diffractometer (Bruker, Billerica, MA, USA) with a Bragg Brentano geometry and monochromatic  $CuK\alpha$  radiation ( $\lambda = 1.541 \text{ \AA}$ ), operated at 40 kV and 30 mA. The X-Ray diffraction patterns were recorder in reflection mode in an angular range of 5° to 60° ( $2\theta$ ), with a step time of 0.5 s and a step size of 0.02°. The crystallinity was calculated according to equation 5 (Aguilar-Pérez *et al.*, 2020).

$$1 - \frac{\text{maximum peak}}{\text{minimum peak}} \times 100 \quad \text{eq. (5)}$$

#### FTIR-ATR spectrophotometry

Attenuated total reflectance infrared (FTIR-ATR) spectra of starch were obtained at room temperature using a Thermo Nicolet model Nexus 670-FTIR spectrometer (Madison, WI). The samples were analyzed in the range of 4000 - 600  $cm^{-1}$ , with 4  $cm^{-1}$  resolution and 100 scans, the OMNIC software was used to obtain the results (Madera-Santana *et al.*, 2016).

### Statistical analysis

Data were presented as average of triplicate measurements  $\pm$  standard deviation. The results obtained in percentage form were transformed to a arcsine to optimize the normality of the data. An analysis of variance (ANOVA) was performed with a completely randomized design (DCA) and a level of significance ( $p \leq 0.05$ ), the Tukey test was applied to determine significant differences between means using the SAS statistical analysis software (version 9.3).

## RESULTS AND DISCUSSION

### Proximate composition analysis

The proximal composition of the potato starch is shown in Table 1. Similar moisture values were reported by Bravo and Chavarría (2020) with 12.6 % for Leona Blanca variety potato starch, while Acosta *et al.* (2018) indicated higher values (16.9 - 20.8 %). Dry starches usually have a humidity that ranges between 6 - 16 %; this variation is due to the environment and the drying process employed, however, the humidity should not exceed 13 %, since high levels can cause microbial damages and deteriorate quality (Moorthy, 2002).

**Table 1.** Proximal composition of residual potato starch.

**Tabla 1.** Composición proximal de almidón de residuos de papa.

Components	Results (%)
Moisture	10.60 $\pm$ 0.14
Ash	0.26 $\pm$ 0.02
Lipids	0.15 $\pm$ 0.02
Protein	1.18 $\pm$ 0.06
Carbohydrate	87.79 $\pm$ 0.16
Amylose	24.35 $\pm$ 6.70

The results obtained in this work for ashes, lipids, proteins, and carbohydrates were similar to those reported in previous studies. In this sense, Bravo and Chavarría (2020) reported a proximal composition of potato starch (Leona Blanca variety) with 0.12 % lipids, 0.35 % proteins and 85.87 % carbohydrates, Pardo *et al.* (2013) mentioned a 0.23 - 0.44 % range for ashes and 0.28 - 0.33 % for protein in potato starch, and Vargas *et al.* (2016) reported values of 0.43, 0.3 and 98.8 % of ashes, lipids, and carbohydrates, respectively, for potato starch (Única variety).

The variation in the proximal composition of starches has been reported between and within botanical species, since they are influenced by various factors such as growth, development conditions of the plant and the variety used, showing a direct effect on interactions with other molecules, resulting in different physicochemical, functional, and microscopic properties (Martínez *et al.*, 2019a; Lemos *et al.*, 2019).

The amylose content was another important parameter evaluated because it allows to categorized starches as, waxy (< 15 %), normal (20 - 35 %) or high (> 40 %) (Gonçalves *et al.*, 2020). In the present study, starch was identified as normal (24.35 % amylose), similar to those reported by Torres *et al.* (2020) and Solarte-Montúfar *et al.* (2019) with ranges of 15.6

- 29.3 % and 24.8 - 26.2 % amylose, respectively, in potato starch of different varieties.

These characterization studies are fundamental since they allow deciding the most promising uses of each starch in the different industrial sectors where it is used, and ruling out those for which its characteristics are undesirable. For example, in the use of starch as a food additive, the amylose-amylopectin ratio influences the clarity or opacity of solutions, amylose also provides greater thermal stability to pastes and also exhibits excellent film-forming properties compared to amylopectin, so in this type of industry a high amylose content becomes a desirable characteristic (Solarte-Montúfar *et al.*, 2019).

### Functional properties

#### Water absorption capacity (WAC)

The obtained water absorption capacity (WAC) of potato starch was 1.0163  $\pm$  0.0078 g g<sup>-1</sup> (101.63  $\pm$  0.77 %), a value close to that reported by Sarifudin *et al.* (2020) with 100 %, meanwhile, Cao and Gao (2020) and Chuiza-Rojas *et al.* (2021), reported a higher water absorption capacity of 1.81 gg<sup>-1</sup> and 1.87 g g<sup>-1</sup>, respectively, for potato starch. Potato starch contains phosphate ester groups that provide a higher WAC and a faster rate of hydration compared to cereals starch, which is reflected in a higher viscosity during cooking. This property indicates the ability of starch to interact with water and to form pastes or gels; in addition, its use as food additive allows determining the texture and quality of food, so that starches that have a high WAC usually intended for this industrial sector, especially as a thickening agent (Solarte-Montúfar *et al.*, 2019; Jiménez-Villalba *et al.*, 2019).

The WAC of starch is influenced by granule size (small granules, characteristic of amylopectin, retain more water than large granules, typical of amylose), and the presence of hydrophilic groups (which have a high-water retention capacity) (Guízar *et al.*, 2008; Babu and Parimalavalli, 2014; Martínez *et al.*, 2015; Sangokunle *et al.*, 2020).

#### Solubility index and swelling power

The starch, subjected to high temperatures and excess of water, show a gelatinization process due to the breaking of the crystalline structure allowing the union of water molecules with the -OH groups of the amylose and amylopectin through hydrogen bonds, promoting the solubility and swelling processes (Soto and Oliva, 2012). The water solubility index is a measure of the amount of amylose that is released from inside the granule when it begins to lose its structure by the effect of water absorption (Huamani-H *et al.*, 2020); the results obtained in the present work are shown in table 2. In this sense, Sindhu *et al.* (2019) reported values similar to those obtained in this study, with 31.32 % for buckwheat starch. Meanwhile, Martínez *et al.* (2015) reported a lower solubility value for potato starch (4.8 - 20.8 %).

An increase in starch solubility index has been reported with increasing temperature (Martínez *et al.*, 2017), however, in the present work the maximum solubility index values

**Table 2.** Solubility index and Swelling power of residual potato starch.  
**Tabla 2.** Índice de solubilidad y poder de hinchamiento de almidón de residuo de papa.

Temperature °C	Solubility index (%)	Swelling power (g g <sup>-1</sup> )
60	42.87 ± 3.95 <sup>a</sup>	2.31 ± 0.11 <sup>c</sup>
70	46.65 ± 0.39 <sup>a</sup>	6.12 ± 0.40 <sup>b</sup>
80	36.52 ± 0.66 <sup>b</sup>	8.24 ± 0.66 <sup>a</sup>
90	30.17 ± 0.31 <sup>c</sup>	8.69 ± 0.45 <sup>a</sup>

were reached between 60 °C and 70 °C, with a decrement at 80 °C and 90 °C. Guizar *et al.* (2008) reported a similar behavior, with maximum solubility index values between 70 - 80 °C, and a subsequent decrease at 90 °C for sweet potato starch, attributed to the fact that when reaching the maximum solubility, the starch components (amylose-amylopectin) begin to interact with each other forming insoluble complexes, which precipitate decreasing the solubility index.

The swelling power indicates the ability of starch granules to hydrate under cooking conditions (Olu-Owolabi *et al.*, 2011) and can be affected by their minor components (lipids, proteins, etc.) that prevent interaction with water, prior treatment, and processing conditions (Solarte-Montúfar *et al.*, 2019). Martínez *et al.* (2015) and Babu and Parimalavalli (2014) reported a swelling power of 11 - 26.9 g g<sup>-1</sup> for potato starch and 3 - 14 g g<sup>-1</sup> for sweet potato starch, respectively, similar to those reported in this work.

As the temperature increases, the intergranular forces of the starch weaken, thus facilitating the penetration of water into the crystalline zone, so that the granules swell and increase in volume. Once the amorphous part is hydrated, the maximum swelling point occurs (Olu-Owolabi *et al.*, 2011; Martínez *et al.*, 2017). The results observed at 80 °C in this work are very close to the final gelatinization temperature (Tf: ~ 90 °C) evaluated by DSC, corroborating that mentioned by Chacón *et al.* (2020), who attribute a direct relationship between solubility index and swelling power with starch gelatinization temperature. It is worth mentioning that various studies have attributed that solubility is mainly affected by amylose content, while amylopectin affects swelling power characteristics (Yadav *et al.*, 2019).

## MORPHOLOGICAL AND OPTICAL ANALYSIS

### Scanning electron microscopy (SEM) and elemental analysis (EDS)

The starch sample showed a wide particle size distribution ranging from 14 to 69 µm, as well as an oval shape with a smooth surface (Figure 1). Conglomerates can be observed as a result of electrostatic charges between large and small particles. In this sense, Morales (2012) mentions a size of 5 to 100 µm for potato starch particles, while Ramírez *et al.* (2017) reported an average size of 27.1 µm.

Both size and shape turn out to be important in the characterization of starches, since they have a great influence on their properties and applications (Jaiswal and Chibbar, 2017), these characteristics are related to amylose and amy-

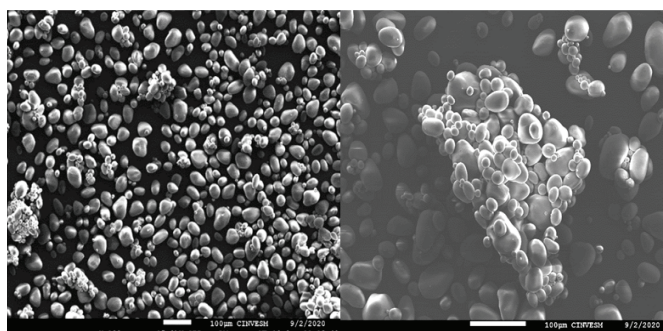


**Figure 1.** Scanning electron microscopy (SEM) of residual potato starch. a) 100X magnification, b) 200X magnification.

**Figura 1.** Microscopía electrónica de barrido (MEB) de almidón de residuo de papa. a) ampliación a 100X b) ampliación a 200X.

lopectin within starch granules, since the amylopectin chains form small oval granules, while amylose tends to form larger granules (Hernández *et al.*, 2017). This is corroborated by Chuiza-Rojas *et al.* (2021) who reported a size of 6.2 µm and a relatively low amylose content of 19.28 % compared to that obtained in this study (24.35 %), which was reflected in larger particles (14 - 69 µm).

Scanning electron microscopy with energy dispersive detector (EDS) allows knowing part of the simple chemical composition of starch (Table 3). The potato starch sample showed a simple composition of 54.39 % carbon, 45.46 % oxygen, and 0.15 % potassium. Bahrami *et al.* (2019) reported a similar chemical composition for potato starch, with 59.31 % carbon and 40.69 % oxygen, while Hernández *et al.* (2017) indicated a composition of 76.43 % carbon and 23.23 % oxygen. The potassium detected in this test is due to the composition of the starch, since the presence of minerals such as calcium, magnesium, sodium, iron, phosphorus, and potassium has been reported (Meaño *et al.*, 2014).

### Dynamic Light Scattering (DLS)

DLS allows to determine the nanometric size of particles such as starch, as well as the size distribution (Ji *et al.*, 2016). In this sense, the DLS results showed colloids with a nanometric size of approximately 120 ± 18.87 nm. The DLS procedure has a sonication step where the conglomerate particles are separated, which allowed measuring the size of the colloids present in the sample. Garcia-Gurrola *et al.* (2019) and Ang *et al.* (2022) reported a similar procedure used for DLS analysis and demonstrated that the increase in particle size is attributed to associations of amylopectin chains that induce a variation in starch properties, such as rheology.

**Table 3.** Elemental composition by EDS of residual potato starch.

**Tabla 3.** Composición elemental por EDS de almidón de residuo de papa.

Element	Weight (%)	Atomic (%)
C <sub>K</sub>	47.11	54.39
O <sub>K</sub>	52.46	45.46
K <sub>K</sub>	0.43	0.15
Total	100.00	100.00

The determination of the starch particles nanometric size resulted interesting, since these are for example, usually used in drug delivery systems (Zhou *et al.*, 2014), however the characteristics that define the use of nanoparticles also consider the distribution in size and surface charge as they affect physical stability and distribution in vivo (Jimenez, 2022).

The polydispersity index (PDI), which shows the colloidal quality of the particles, was  $0.3028 \pm 0.12$ , showing the starch obtained a monodispersed distribution (narrow size distribution) according to previous reports which showed that values less than 0.7 indicate a monodisperse distribution and those in the range of 0.7 to 1 indicate low quality with a large size distribution (Lancheros *et al.*, 2014; García-Gurrola *et al.*, 2019; Dong *et al.*, 2021). Sana *et al.* (2019) reported a particle size for corn starch of 175 to 248 nm with a PDI of 0.2 to 0.3 and Naderizadeh *et al.* (2018) indicated a particle size of 230 to 240 nm and PDI of 0.26 for potato starch particles, both studies showed similar PDI values to that obtained in the present study.

The zeta potential is indicative of the magnitude of electrostatic repulsion/attraction between particles that influence the stability of the colloid, the value obtained was  $6.14 \pm 0.41$  mV, indicating an unstable suspension ( $\pm 0 - 10$  mV); since this superficial charge is close to zero, the particles are considered neutral with a tendency to form aggregations and precipitate. The zeta potential is an important tool when making formulations, since stability tests are shortened by predicting it, reducing time and costs, in addition to improving the useful life and helping to understand the state of the surface of a nanoparticle (Jeong and Shin, 2018; Ahmad *et al.*, 2020). Previous work has reported zeta potential in this range, Chavez da Silva *et al.* (2017) mentioned a value of -8.67 mV and Haaj *et al.* (2014) pointed out values of 3 mV, considering that suspended solids have a neutral charge so close to zero. The variability of the zeta potential of colloids or suspended particles are influenced by the chemical nature of the polymer, pH, solvent, and the stabilizing agent (Piña-Barrera *et al.*, 2021).

## Color

Starch color is an important quality parameter, which influences the acceptability of the product by consumers (Too *et al.*, 2022). In this study the colorimetric analysis of starch showed a medium luminosity ( $40.42 \pm 0.44$ ), since sodium metabisulfite or any other antioxidant that favored the whiteness of the starch was not used in the extraction. The values of the parameters  $a^*$  ( $0.06 \pm 0.02$ ) and  $b^*$  ( $2.86 \pm 0.09$ ) with an inclination to reddish and yellow color, respectively, indicate a tendency to neutral color (Martínez *et al.*, 2019b). Verma *et al.* (2018) reported similar values (0.16 for  $a^*$  and 2.58 for  $b^*$ ), however, they mentioned a higher luminosity (98.81). Likewise, Kumar *et al.* (2020) reported a luminosity of 96.68 and values of -0.14 and 1.89 for parameters  $a^*$  and  $b^*$ , respectively, in both cases for potato starch.

## Thermal analysis

### Differential Scanning Calorimetry (DSC)

The DSC thermograms (Figure 2) allowed us to observe the changes that occurred in the potato starch gelatinization process, which presented an initial temperature ( $T_0$ ) of said process to  $61.78$  °C, while the maximum temperature ( $T_p$ ) was observed to  $64.45$  °C and the final temperature ( $T_f$ ) was recorded at around  $90$  °C, and the enthalpy of gelatinization ( $\Delta H$ ) was  $10.96$  J/g. These results are similar to those reported by Gonçalves *et al.* (2020), with values of  $T_0$  ( $55.1$  °C and  $58.2$  °C),  $T_p$  ( $59$  °C and  $62$  °C) and  $T_f$  ( $71.4$  °C and  $74.4$  °C) and a  $\Delta H$  of  $11.8$  J/g and  $12.7$  J/g, for recovered and commercial potato starch, respectively. On the other hand, Alvani *et al.* (2011) reported values of  $T_0$  ( $58.7$  °C to  $62.5$  °C),  $T_p$  ( $62.5$  °C to  $66.1$  °C) and  $T_f$  ( $68.7$  °C to  $72.3$  °C) and  $\Delta H$  that ranged between  $15.1$  and  $18.4$  J/g, for potato starches.

In the present work, an endothermic peak was observed at  $114.56$  °C, attributed to the dissociation of the amylose-lipid complex. In this sense, Genkina *et al.* (2014) reported a peak around  $95$  °C for corn starch and mentioned that the fusion of these complexes is a reversible process, contrary to the phase transition of amylopectin. These changes in the transition temperature of starch are attributed to its

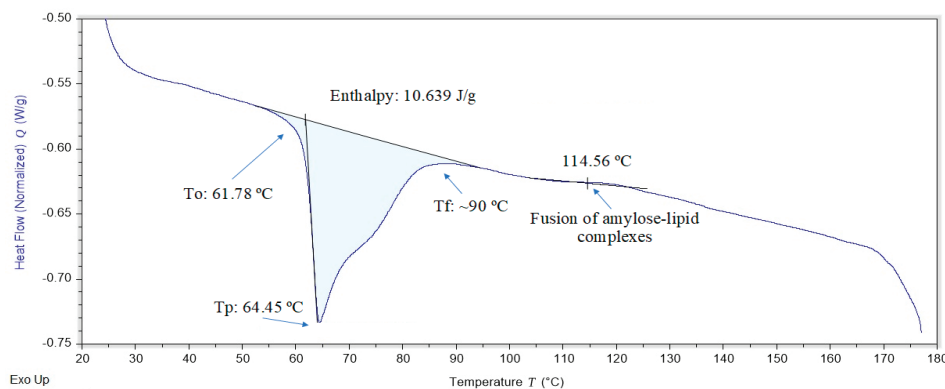


**Figure 2.** Differential scanning calorimetry (DSC) of residual potato starch.

**Figura 2.** Calorimetría diferencial de barrido (CDB) de almidón de residuo de papa.

botanical source, its crystallinity and composition, since the amylose content is negatively correlated (Li *et al.*, 2017; Han *et al.*, 2019). Furthermore, lipids are a determining factor, since their presence results in a gelatinization process at higher temperatures (Alvani *et al.*, 2011).

On the other hand, enthalpy values ( $\Delta H$ ) are positively correlated with crystal concentration, being an indicator of the loss of molecular order. Then, low enthalpy values indicate that less energy is required to start the gelatinization process. Enthalpy is also related to the shape, size, and presence of phosphate esters in starch granules (Alvani *et al.*, 2011; Li *et al.*, 2017; Li *et al.*, 2020; Zhang *et al.*, 2021).

### Thermogravimetric analysis (TGA/DTGA)

Thermogravimetric analysis (TGA) and differential thermogravimetric analysis (DTGA) of potato starch describe its thermal stability (Figure 3). Starch shows three zones of weight loss within a temperature range of 20 - 500 °C. The first mass loss of 4.09 % detected at 49.22 °C is attributed to the evaporation of water, the other two regions comprised at 288.17 °C and 474.90 to 482.25 °C, represent the greater mass loss of 53.2 % and 96.17 %, respectively, due to the thermal degradation of starch and proteins (Thakur *et al.*, 2021; Gui *et al.*, 2022), the residual mass (ash) was detected at 600 °C (0.82 %). These results are similar to those reported by Gui *et al.* (2022), with two mass loss zones between 30 - 150 °C and 150 - 750 °C. Similarly, Li *et al.* (2022) pointed out two degradation zones in the same temperature ranges, specifically at 70 °C and 300 °C, in both cases for potato starch.

### Structural analysis

#### NMR spectra

Figure 4 shows the  $^{13}\text{C}$  NMR spectrum of potato starch in the range of - 20 to 230 ppm. The NMR spectrum detected

the presence of five peaks between 60 - 105 ppm. The peak recorded around 60 ppm is due to carbon 6 of the glucose unit, while the wide peak observed between 70 and 80 ppm is related to carbons 2, 3 and 5, C4 was detected at 80 ppm, while carbon 1 presents two peaks around 100 of ppm, thus corroborating the structure of the starch monomer (glucose) (Thérien-Aubin *et al.*, 2007; Šoltýs *et al.*, 2019).

The C1 resonance peak provides information about the conformation of the starch molecule, crystallinity, and double-helix symmetry. For type A crystallinity, the C1 resonance presents three peaks at 102, 101 and 100 ppm, whilst, type B (characteristic of potato starch) presents two peaks at 101 and 100 ppm, as observed in this study. According to Meaño *et al.* (2016) the amylose content for type B starches (25 - 30 %) is higher compared to type A, as is the size of the granules, which agrees with the results obtained in this investigation. The broad C1 resonance peak around 103 - 104 ppm is typical of single helices, both in amorphous and crystalline V phase, suggesting a higher proportion of short amylopectin chains attributed to degradation (Thérien-Aubin *et al.*, 2007; Pardo *et al.*, 2013; Li *et al.*, 2017).

### X-ray diffraction (XRD)

X-ray diffraction of potato starch was performed to examine its amorphous, semi-crystalline or crystalline structure. X-ray patterns identified crystalline structures, characteristic of amylopectin (Pardo *et al.*, 2013), which can classify starch into types A-C. Type A crystallinity starch shows two strong diffraction peaks between 15° and 23° and a doublet at 17° and 18°, type B crystallinity produces a strong diffraction peak at 17° and low intensity peaks between 15 - 24°, while type C is a mixture of A and B (Ma *et al.*, 2022).

As shown in Figure 5, the diffraction showed type B crystallinity patterns typical of potato starch, with a strong

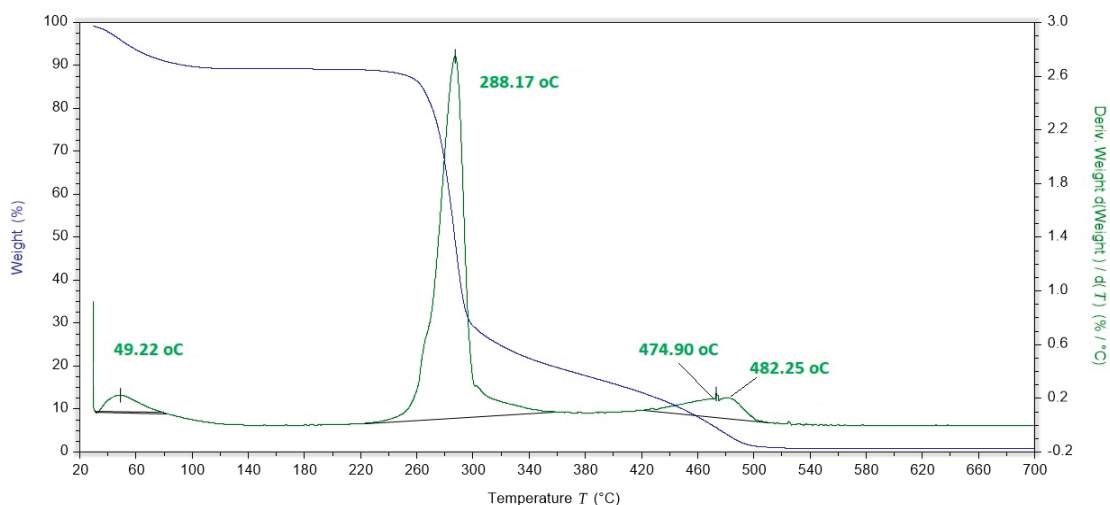


**Figure 3.** Thermogravimetric analysis (TGA) and curves of thermogravimetric differential analysis (DTGA) of residual potato starch.

**Figura 3.** Análisis termogravimétrico (ATG) y curvas de análisis termogravimétrico diferencial (ATD) de almidón de residuo de papa.

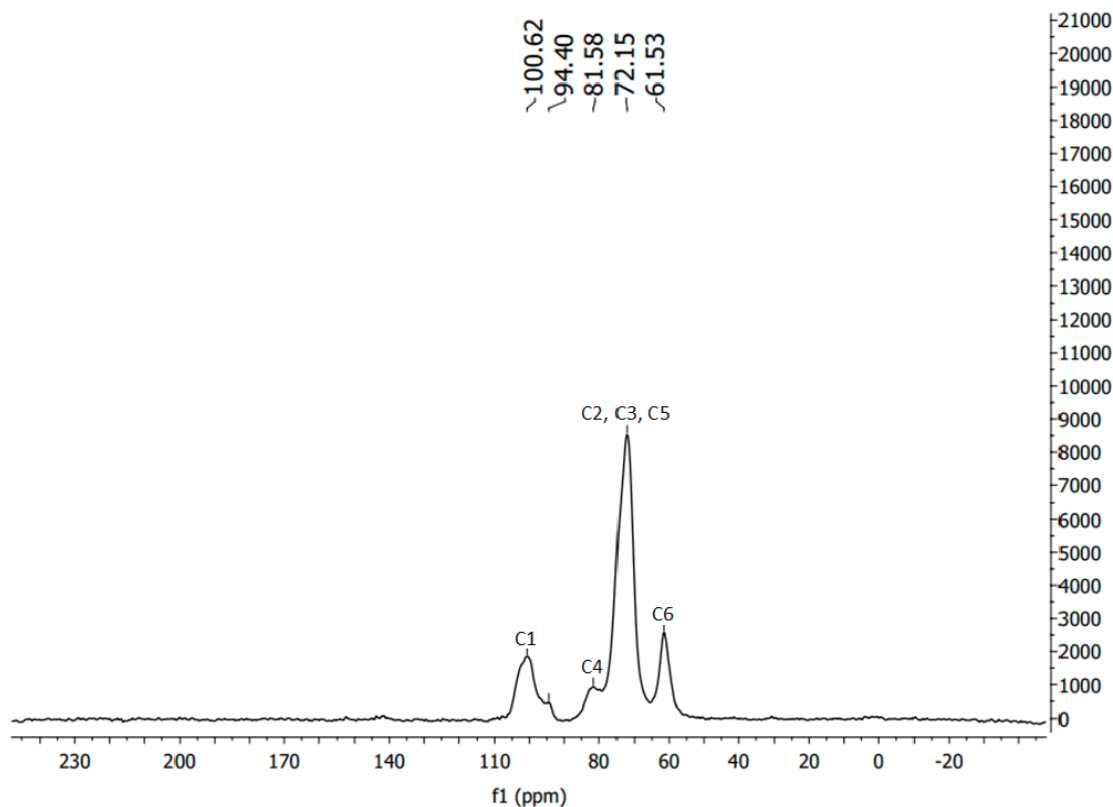


**Figure 4.** Nuclear magnetic resonance (NMR) of residual potato starch.  
**Figura 4.** Resonancia magnética nuclear (RMN) de almidón de residuo de papa.

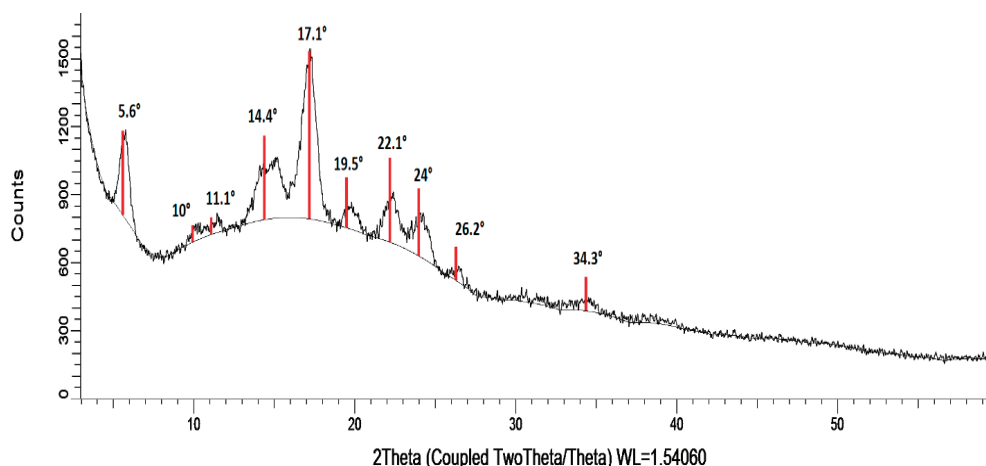


**Figure 5.** X-ray diffraction (XRD) spectrum of residual potato starch.  
**Figura 5.** Espectros de difracción de rayos X (DRX) de almidón de residuo de papa.

diffraction peak at  $17.1^\circ$  and low intensity peaks between a range of  $5.6 - 26.2^\circ$ , corroborating the results obtained by NMR. The degree of starch crystallinity was estimated at 34.73 %, values similar to those reported by Núñez-Santiago *et al.* (2011) and Gui *et al.* (2022) who reported 32.3 % and 31.5 % crystallinity, respectively, for commercial potato starch in both cases.

#### FTIR-ATR spectrophotometry

The glucose (starch monomer) structure previously detected with NMR, was corroborated with the detection of their functional groups by FTIR-ATR spectrophotometry (Figure 6). Signals were observed at wave numbers of 763, 858 and  $929\text{ cm}^{-1}$ , which are attributed to the stretching of the ether groups (C-O-C) of the glucose ring, in addition, the band

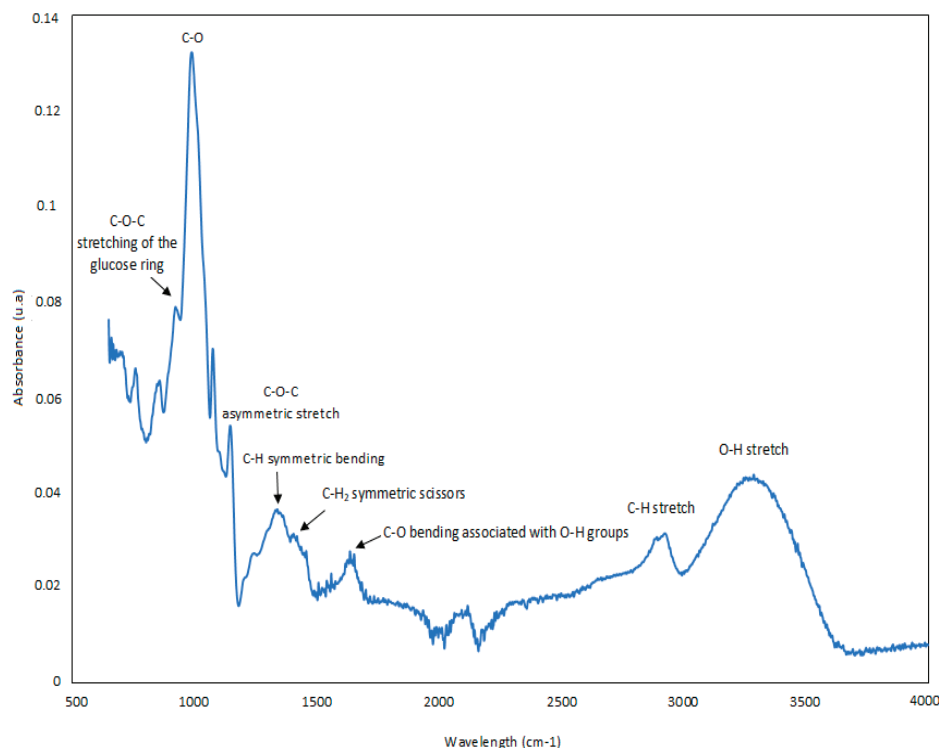


**Figure 6.** FTIR-ATR spectrum of residual potato starch.  
**Figura 6.** Espectros FTIR-ATR de almidón de residuo de papa.

observed between 993-1082  $\text{cm}^{-1}$  was due to the C-O bonds stretching. The presence of an absorption band around 1157  $\text{cm}^{-1}$  indicated an asymmetric stretching of the C-O-C groups. Symmetric double vibration of C-H bonds and symmetric deformation of  $\text{CH}_2$  groups were observed at wavelengths 1381 and 1437  $\text{cm}^{-1}$ , respectively. The absorption band around 3300 - 3600 and 2900  $\text{cm}^{-1}$  indicated the presence of hydroxyl functional groups (-OH) and C-H bonds, respectively. The C-O bending associated with the -OH groups showed an absorbance peak around 1648  $\text{cm}^{-1}$ . The absorbance peak at 1415  $\text{cm}^{-1}$  implies the presence of a symmetric scissors of the  $\text{CH}_2$  groups. The unusual  $\text{CO}_2$  peak (2358  $\text{cm}^{-1}$ ) observed in the starch IR spectrum could be the result of the measurement conditions (Torres *et al.*, 2015; Abdullah *et al.*, 2018).

## CONCLUSIONS

The extraction process has influence on the starch color parameters, mainly in the luminosity parameter. The NMR and XRD-ray diffraction allowed the identification of the potato starch crystallinity as type B. The SEM-EDS revealed particles of oval shape and the formation of conglomerates, with an elemental composition of carbon, oxygen, and potassium, and DLS showed a narrow size distribution with a zeta potential close to zero, considering the particles in suspension as neutral. In addition, the FTIR-ATR spectrum corroborated the chemical structure of starch, and the TGA thermogram showed the presence of different stages of weight loss, while the DSC thermogram showed the behavior of the

starch gelatinization process, whose temperature showed a direct relationship with solubility and swelling power. The results found in the present work show the relationship between the chemical components of potato starch and its thermal, structural, and morphological behavior, which are important due to the wide range of applications attributed to this product. Residual potato is an excellent source of high-quality starch due to its physicochemical, thermal, and structural characteristics, resulting in a good alternative for the recycling of residual potato from the chips industry in Mexico. In addition, the use of this residual potato presents an excellent alternative to solve the environmental impact of agroindustrial waste.

## ACKNOWLEDGMENTS

SEM-EDS, TGA, DSC, DLS and XRD measurements were carried out at LANNBIO Cinvestav Merida, with the support of the FOMIX-Yucatan 2008-108160, CONACYT LAB-2009-01-123913, 292692, 294643, 188345 and 204822 projects. To Drs. Patricia Quintana Owen, William Santiago Gonzalez and Victor Rejon M, for the support provided in the different characterization analyzes of the starch.

## REFERENCES

- Abdullah, A.H.D., Chalimah, S., Primadona, I., and Hanantyo, M.H.G. 2018. Physical and chemical properties of corn, cassava, and potato starches. IOP Conference Series: Earth and Environmental Science. 160:012003. doi: 10.1088/1755-1315/160/1/012003

- Acosta, J., Gomajoa, H., Benavides, Y., Charfuelan, A., and Valenzuela, F. 2018. Evaluación del almidón de papa (*Solanum tuberosum*) en la obtención de bioplástico. Bionatura Conference Series 1. doi: 10.21931/RB/CS/2018.01.01.2
- Acosta-Ferreira, S., Castillo, O.S., Madera-Santana, J.T., Mendoza-García, D.A., Núñez-Colín, C.A., Grijalva-Verdugo, C., Villa-Lerma, A.G., Morales-Vargas, A.T., and Rodríguez-Núñez, J.R. 2020. Production and physicochemical characterization of chitosan for the harvesting of wild microalgae consortia. Biotechnology Reports. 28: e00554. doi: 10.1016/j.btre.2020.e00554
- Aguiar-Perez, D., Vargas-Coronado, R., Cervantes-Uc, J.M., Rodríguez-Fuentes, N., Aparicio, C., Covarrubias, C., Alvarez-Perez, M., Garcia-Perez, V., Martínez-Hernandez, M., and Cauch-Rodríguez, J.V. 2020. Antibacterial activity of a glass ionomer cement doped with copper nanoparticles. Dental Materials Journal. 39: 389-396. doi:10.4012/dmj.2019-046
- Ahmad, M., Gani, A., Hassan, I., Huang, Q., and Shabbir, H. 2020. Production and characterization of starch nanoparticles by mild alkali hydrolysis and ultra-sonication process. Scientific Reports. 10: 3533. doi:10.1038/s41598-020-60380-0
- Alvani, K., Qi, X., Tester, R.F., and Snape, C.E. 2011. Physicochemical properties of potato starches. Food Chemistry. 125: 958-965. doi: 10.1016/j.foodchem.2010.09.088
- Ang, C.L., Matia-Merino, L., Sims, I.M., Sargison, L., Edwards, P.J., Lim, K., and Goh, K.K.T. 2022. Characterisation of de-structured starch and its shear-thickening mechanism. Food Hydrocolloids. 132: 107864. doi: 10.1016/j.foodhyd.2022.107864
- Babu, A.S., and Parimalavalli, R. 2014. Effect of starch isolation method on properties of sweet potato starch. The Annals of the University of Dunarea de Jos of Galati. Fascicle VI. Food Technology, 38:48.
- Bahrami, M., Amiri, M.J., and Bagheri, F. 2019. Optimization of the lead removal from aqueous solution using two starch based adsorbents: Design of experiments using response surface methodology (RSM). Journal of Environmental Chemical Engineering. 7: 102793. doi: 10.1016/j.jece.2018.11.038
- Basiak, E., Lenart, A., and Debeaufort, F. 2017. Effect of starch type on the physico-chemical properties of edible films. International Journal of Biological Macromolecules. 98: 348-356. doi: 10.1016/j.ijbiomac.2017.01.122
- Bravo, A.F.V., and Chavarría, M.A. C. 2020. Extracción y caracterización del almidón de papa (*Solanum tuberosum*) variedad Leona Blanca. Revista Ciencia y Tecnología El Higo. 10: 26-34.
- Calvache, M., Potosí, S., and Rodríguez, A. 2022. Sostenibilidad gastronómica: Aprovechamiento de subproductos derivados de cadena productiva de la papa variedad *Diacol Capiro*. Revista Científica Ciencias Naturales y Ambientales. 16: 389-397.
- Cao, M., and Gao, Q. 2020. Effect of dual modification with ultrasonic and electric field on potato starch. International Journal of Biological Macromolecules. 150: 637-643. doi: 10.1016/j.ijbiomac.2020.02.00
- Chacón, W.D.C., Dos Santos Lima, K.T., Valencia, G.A., and Henao, A.C.A. 2020. Physicochemical properties of potato starch nanoparticles produced by anti-solvent precipitation. Starch-Stärke. 73: 2000086. doi:10.1002/star.202000086
- Chavez da Silva N.M., Cruz C.P.R., Druzian J.I., Fakhouri F.M., Lima F.R.L., and Cabral de Albuquerque E.C. 2017. PBAT/TPS Composite films reinforced with starch nanoparticles produced by ultrasound. International Journal of Polymer Science. 4308261. doi:10.1155/2017/4308261
- Chuiza-Rojas, M.R., Haro-Velasteguí, C.V., and Brito-Moína, H.L. 2021. Identificación de las variables de proceso óptimas para la producción del almidón de papa china (*Colocasia esculenta*). Dominio de las Ciencias. 7: 41. doi: 10.23857/dc.v7i1.1680
- Devaux, A., Goffart, J. P., Kromann, P., Andrade-Piedra, J., Polar, V., and Hareau, G. 2021. The potato of the future: opportunities and challenges in sustainable Agri-food Systems. Potato Research. 64: 681-720. doi: 10.1007/s11540-021-09501-4
- Dong, H., Chen, L., Zhang, Q., Gao, J., and Vasanthan, T. 2021. Optimization of processing parameters to produce nanoparticles prepared by rapid nanoprecipitation of pea starch. Food Hydrocolloids. 121: 106929. doi: 10.1016/j.foodhyd.2021.106929
- Dupuis, J., and Liu, Q. 2019. Potato starch: A review of physicochemical, functional and nutritional properties. American Journal of Potato Association. 96: 127-138. doi: 10.1007/s12230-018-09696-2
- FAOSTAT. 2020. Food and Agriculture Organization of the United Nations. Statistics division. Recuperado de: <https://www.fao.org/faostat/es/#data/.02/11/2020>.
- García-Gurrola, A., Rincón, S., Escobar-Puentes, A.A., Zepeda, A., Francisco Pérez-Robles, J., and Martínez-Bustos, F. 2019. Synthesis and succinylation of starch nanoparticles by means of a single step using sonochemical energy. Ultrasonics Sonochemistry. 56: 458-465. doi: 10.1016/j.ultsonch.2019.04.035
- Genkina, N.K., Kozlov, S.S., Martirosyan, V.V., and Kiseleva, V.I. 2014. Thermal behavior of maize starches with different amylose/amylopectin ratio studied by DSC analysis. Starch - Stärke. 66: 700-706. doi:10.1002/star.201300220
- Gómez, A.F.P., and González-García, G. 2018. Síntesis y caracterización de un nuevo complejo hexacoordinado neutro de estaño (IV) con ligante O,N,N,O donador tipo salen. Jóvenes en la ciencia. 4:832-836.
- Gonçalves, I., Lopes, J., Barra, A., Hernández, D., Nunes, C., Kapusniak, K., Kapusniak, J., Evtyugin, D.V., Lopes, S.J.A., Ferreira, P., and Coimbra, M.A. 2020. Tailoring the surface properties and flexibility of starch-based films using oil and waxes recovered from potato chips byproducts. International Journal of Biological Macromolecules. 163: 251-259. doi: 10.1016/j.ijbiomac.2020.06.231
- González-Cuello, R. E., Paternina, L., and Carrillo, A. 2016. Biopelículas terciarias: fuerza de ruptura y efecto sobre la vida útil de cortes de tilapia negra (*Oreochromis niloticus*). Información tecnológica. 27: 33-40. doi: 10.4067/S0718-07642016000100005
- Gui, Y., Zou, F., Zhu, Y., Li, J., Wang, N., Guo, L., and Cui, B. 2022. The structural, thermal, pasting and gel properties of the mixtures of enzyme-treated potato protein and potato starch. LWT. 154: 112882. doi: 10.1016/j.lwt.2021.112882
- Guízar, M.A., Montañez, S.J.L., and García, R.I. 2008. Parcial caracterización de nuevos almidones obtenidos del tubérculo de camote del cerro (*Dioscorea* spp). Revista Iberoamericana de Tecnología Postcosecha. 9: 81-88.
- Haaj, S.B., Magnin, A., and Boufi, S. 2014. Starch nanoparticles produced via ultrasonication as a sustainable stabilizer in pickering emulsion polymerization. RSC Advances. 4: 42638-42646.

- Han, H., Hou, J., Yang, N., Zhang, Y., Chen, H., Zhang, Z., Shen, Y., Huang, S., and Guo, S. 2019. Insight on the changes of cassava and potato starch granules during gelatinization. *International Journal of Biological Macromolecules*. 126, 37-43. doi: 10.1016/j.ijbiomac.2018.12.201
- Hernández, J.E., Medina, O.J., Hernández, A.L., and Cocha, P.M. 2017. Oxidación y caracterización fisicoquímica de almidón de sagú "*Marantha Arundinacea*" para la elaboración de bioplástico. *Fuentes, el reventón energético*. 15: 19-26. doi: 10.18273/revfue.v15n1-2017002
- Hoover, R., and Ratnayake, W.S. 2001. Determination of total amylose content of starch. *Current Protocols in Food Analytical Chemistry*. E2.3.1-E2.3.5. doi: 10.1002/0471142913.fae0203s00
- Huamani-H, A.L., Ponce-Ramírez, J.C., and Málaga-Juárez, J. 2020. Optimización del proceso de cocción de quinua utilizando el diseño 3k y la función de deseabilidad: Grado de gelatinización, índice de absorción de agua, índice de solubilidad y desprendimiento de cotiledones. *Scientia Agropecuaria*. 11: 381-390. doi: 10.17268/sci.agropecu.2020.03.10
- Jagadeesan, S., Govindaraju, I., and Mazumder, N. 2020. An insight into the ultrastructural and physicochemical characterization of potato starch: a review. *American Journal of Potato Research*. 97: 464-476. doi: 10.1007/s12230-020-09798-w
- Jaiswal, S., and Chibbar, R.N. 2017. Amylopectin small chain glucans form structure fingerprint that determines botanical origin of starch. *Carbohydrate Polymers*. 158: 112-123. doi: 10.1016/j.carbpol.2016.11.059
- James, C.S. 1999. *Analytical Chemistry of Foods*. Second Edition, ASPEN Publishers. New York.
- Jeong, O., and Shin, M. 2018. Preparation and stability of resistant starch nanoparticles, using acid hydrolysis and cross-linking of waxy rice starch. *Food Chemistry*. 256: 77-84. doi: 10.1016/j.foodchem.2018.02.098
- Ji, G., Luo, Z., Xiao, Z., and Peng, X. 2016. Synthesis of starch nanoparticles in a novel microemulsion with two ILS substituting two phases. *Journal of Materials Science*. 51: 7085-7092. doi: 10.1007/s10853-016-9952-1
- Jiménez-Villalba, K., Arrieta-Banquet, L., Salcedo-Mendoza, J., and Contreras-Lozano, K. 2019. Caracterización de harinas y almidones de batatas (*Ipomoea batatas* Lam.) de la costa caribe colombiana. *Revista U.D.C.A Actualidad y Divulgación Científica*. 22: e1185. doi: 10.31910/rudca.v22.n1.2019.1185
- Jiménez, H. L. G. 2022. Desarrollo, aplicaciones y desafíos de la nanomedicina. *Infodir*. e1216.
- Kirk, R.S., and Sawyer, R. 1991. *Pearson's Composition and Analysis of Food*. 9th Edition. Longman Scientific & Technical, England.
- Kowsik, P.V., and Mazumder, N. 2018. Structural and chemical characterization of rice and potato starch granules using microscopy and spectroscopy. *Microscopy Research and Technique*. 81: 1533-1540. doi: 10.1002/jemt.23160
- Kumar, Y., Singh, L., Sharanagat, V. S., Patel, A., and Kumar, K. 2020. Effect of microwave treatment (low power and varying time) on potato starch: Microstructure, thermo-functional, pasting and rheological properties. *International Journal of Biological Macromolecules*. 155: 27-35. doi: 10.1016/j.ijbiomac.2020.03.17
- Lancheros, R.J., Beleño, J.A., Guerrero, C.A., and Godoy-Silva, R.D. 2014. Producción de nanopartículas de PLGA por el método de emulsión y evaporación para encapsular N-Acetilcisteína (NAC). *Universitas Scientiarum*. 19: 161-168.
- Lemos, P.V.F., Barbosa, L.S., Ramos, I.G., Coelho, R.E., and Druzian, J.I. 2019. Characterization of amylose and amylopectin fractions separated from potato, banana, corn, and cassava starches. *International Journal of Biological Macromolecules*. 132: 32-42. doi: 10.1016/j.ijbiomac.2019.03.086
- Li, C., Oh, S.G., Lee, D.H., Baik, H.W., and Chung, H.J. 2017. Effect of germination on the structures and physicochemical properties of starches from brown rice, oat, sorghum, and millet. *International Journal of Biological Macromolecules*. 105: 931-939. doi: 10.1016/j.ijbiomac.2017.07.123
- Li, J., Yang, N., Tang, J., Gui, Y., Zhu, Y., Guo, L., and Cui, B. 2022. The characterization of structural, thermal, pasting and gel properties of the blends of laccase-and tyrosinase-treated potato protein and starch. *LWT*. 153: 112463. doi: 10.1016/j.lwt.2021.112463
- Li, Z., and Wei, C. 2020. Morphology, structure, properties and applications of starch ghost: a review. *International Journal of Biological Macromolecules*. 163: 2084-2096. doi: 10.1016/j.ijbiomac.2020.09.077
- Ma, Y., Zhao, H., Ma, Q., Cheng, D., Zhang, Y., Wang, W., Wang, J., and Sun, J. 2022. Development of chitosan/potato peel polyphenols nanoparticles driven extended-release antioxidant films based on potato starch. *Food Packaging and Shelf Life*. 31: 100793. doi: 10.1016/j.fpsl.2021.100793
- Madera-Santana, T. J., Meléndrez, R., González-García, G., Quintana-Owen, P., and Pillai, S.D. 2016. Effect of gamma irradiation on physicochemical properties of commercial poly(lactic acid) clamshell for food packaging. *Radiation Physics and Chemistry*. 123: 6-13. doi: 10.1016/j.radphyschem.2016.02.001
- Maniglia, B.C., Castanha, N., Le-Bail, P., Le-Bail, A., and Augusto, P.E. 2020. Starch modification through environmentally friendly alternatives: a review. *Critical Reviews in Food Science and Nutrition*. 61: 2482-2505. doi: 10.1080/10408398.2020.1778633
- Martínez, J., Hernández, J., and Arias, A. 2017. Physicochemical and functional properties of white and brown rice (*Oryza sativa* L) starch. *Alimentos Hoy*. 25: 15-30.
- Martínez, P., Málaga, A., Betalueluz, I., Ibarz, A., and Velezmoro, C. 2015. Caracterización funcional de almidones nativos obtenidos de papas (*Solanum phureja*) nativas peruanas. *Scientia Agropecuaria*. 6: 291-301. doi: 10.17268/sci.agropecu.2015.04.06
- Martínez, P., Peña, F., Gómez, Y., Vargas, G., and Velezmoro, C. 2019a. Propiedades físicoquímicas, funcionales y estructurales de almidones nativos y acetilados obtenidos a partir de la papa (*Solanum tuberosum*) var. 'única'. *Revista de la Sociedad Química del Perú*. 85: 338-351.
- Martínez, P., Peña, F., Bello-Pérez, L. A., Núñez-Santiago, C., Yee-Madeira, H., and Velezmoro, C. 2019b. Physicochemical, functional and morphological characterization of starches isolated from three native potatoes of the Andean region. *Food chemistry: X*. 2: 100030. doi: 10.1016/j.fochx.2019.100030
- Meaño, C.N., Ciarfella, P.A.T., and Dorta, V.A.M. 2014. Evaluación de las propiedades químicas y funcionales del almidón nativo de ñame congo (*Dioscorea bulbifera* L.) para predecir sus posibles usos tecnológicos. *Saber*. 26: 182-188.

- Meaño, C.N., Ciarfella, P.A.T., and Dorta, V.A.M. 2016. Morphological characterization and viscoamulograph ic profile of native starch of Congo yam (*Dioscorea bulbifera* L.). *Saber*. 28: 250-256.
- Mejía, M.G., and Castellanos, S. J. A. 2018. Costos de producción y rentabilidad del cultivo de la papa en Zacapoaxtla, Puebla. *Revista mexicana de ciencias agrícolas*. 9: 1651-1661. doi: 10.29312/remexca.v9i8.1721
- Moorthy, S.N. 2002. Physicochemical and functional properties of tropical tuber starches: A review. *Starch-Stärke*. 54: 559-592. doi:10.1002/1521-379x(200212)54:12<559::aid-star2222559>3.0.co;2-f
- Morales, O.A.F. 2012. Fitogeografía e industrialización del almidón de pituca (*Colocasia esculenta*). *Espacio y Desarrollo*. 24: 97-117.
- Naderizadeh, S., Shakeri, A., Mahdavi, H., Nikfarjam, N., and Taheri Qazvini, N. 2018. Hybrid nanocomposite films of starch, poly (vinyl alcohol) (PVA), starch nanocrystals (SNCs), and montmorillonite (Na-MMT): Structure-properties relationship. *Starch – Stärke*. 1800027. doi: 10.1002/star.201800027
- Núñez-Santiago, M.C., García-Suárez, F.J., Gutierrez-Meraz, F., Sánchez-Rivera, M.M., and Bello-Pérez, L.A. 2011. Some intrinsic and extrinsic factors of acetylated starches: morphological, physicochemical and structural characteristics. *Revista Mexicana de Ingeniería Química*. 10: 501-512.
- NOM-F-68-S-1980. Alimentos Determinación de Proteínas. Recuperado de: [http://dof.gob.mx/nota\\_detalle.php?codigo=4858024&fecha=04/08/1980.09/11/2021](http://dof.gob.mx/nota_detalle.php?codigo=4858024&fecha=04/08/1980.09/11/2021).
- Olu-Owolabi, B.I., Afolabi, T.A., and Adebowale, K.O. 2011. Pasting, thermal, hydration, and functional properties of annealed and heat-moisture treated starch of sword bean (*Canavalia gladiata*). *International Journal of Food Properties*. 14: 157-174. doi: 10.1080/10942910903160331
- Ortega, J. G., and Hector, A. B. 2021. Estado de arte del cultivo de papa para el consumo de papa prefrita congelada (PPFC) en el Ecuador. *Revista Latinoamericana de la Papa*. 25: 42-56. doi: 10.37066/ralap.v25i2.431
- Pardo, C.O.H., Castañeda, J.C., and Ortiz, C.A. 2013. Caracterización estructural y térmica de almidones provenientes de diferentes variedades de papa. *Acta Agronómica*. 62: 289-295.
- Piña-Barrera, A.M., Ramírez Pérez, M.S., Álvarez Román, R., Báez González, J.G., Amaya Guerra, C.A., and Galindo Rodríguez, S.A. 2021. Recubrimiento comestible a base de alginato en combinación con eugenol nanoencapsulado y su efecto conservador en la vida útil de jitomate (*Solanum lycopersicum*). *Biotecnía*. 23: 133-141. doi: 10.18633/biotecnía.v23i3.1477
- Quintero, M.L.P., Martínez, C.Y., Velasco, M.J.A., Arévalo, R.A., Muñoz, Y.A. and Urbina, S. N.A. 2015. Evaluación de residuos de papa, yuca y naranja para la producción de etanol en cultivo discontinuo utilizando *Saccharomyces cerevisiae*. *Revista ION*. 28: 43-53.
- Ramírez, I.H., Castro-Rosas, J., Gómez-Aldapa, C.A., Cortés, R.N.F., and Marín, M.L.R. 2017. Estudio de las propiedades fisicoquímicas y funcionales de mezclas de almidón de papa y almidón de maíz ceroso. *Boletín de Ciencias Agropecuarias del ICAP*. 3. doi:10.29057/icap.v3i6.2447
- Rodríguez-Núñez, J.R., Madera-Santana, T.J., Sánchez-Machado, D. I., López-Cervantes, J., and Soto, V.H. 2014. Chitosan/hydrophilic plasticizer-based films: preparation, physicochemical and antimicrobial properties. *Journal of Polymers and the Environment*. 22: 41-51. doi: 10.1007/s10924-013-0621-z
- Sana, S., Boodhoo, K., and Zivkovic, V. 2019. Production of starch nanoparticles through solvent-antisolvent precipitation in a spinning disc reactor. *Green Processing and Synthesis*. 8: 507-515. doi: 10.1515/gps-2019-0019
- Sánchez-Castelblanco, E. M., and Heredia-Martín, J. P. 2020. Evaluación de residuos de cáscaras de papa como sustrato para la producción de amilasas a partir de *Bacillus amyloliquefaciens* A16. *Revista de la Academia Colombiana de Ciencias Exactas, Físicas y Naturales*. 44: 794-804. doi: 10.18257/raccefyn.1122
- Sangokunle, O.O, Sathe, S.K., and Singh, P. 2020. Purified starches from 18 pulses have markedly different morphology, oil absorption and water absorption capacities, swelling power, and turbidity. *Starch-Stärke*. 72: 2000022. doi: 10.1002/star.202000022
- Sarifudin, A., Keeratiburana, T., Soontaranon, S., Tangsathitkulchai, C., and Tongta, S. 2020. Pore characteristics and structural properties of ethanol-treated starch in relation to water absorption capacity. *LWT*. 129: 109555. doi: 10.1016/j.lwt.2020.109555
- Sattari, M., Fathi, M., Daei, M., Erfan-Niya, H., Barar, J., and Entezami, A.A. 2017. Thermoresponsive graphene oxide – starch micro/nanohydrogel composite as biocompatible drug delivery system. *BiolImpacts*. 7: 167-175. doi:10.15171/bi.2017.20
- Šimková, D., Lachman, J., Hamouz, K., and Vokál, B. 2013. Effect of cultivar, location and year on total starch, amylose, phosphorous content and starch grain size of high starch potato cultivars for food and industrial processing. *Food Chemistry*, 141: 3872-3880. doi: 10.1016/j.foodchem.2013.06.080
- Sindhu, R., Devi, A., and Khatkar, B.S. 2019. Physicochemical, thermal and structural properties of heat moisture treated common buckwheat starches. *Journal of Food Science and Technology*. 56: 2480-2489. doi: 10.1007/s13197-019-03725-6
- Solarte-Montúfar, J.G., Díaz-Murangal, A.E., Osorio-Mora, O., and Mejía-España, D.F. 2019. Propiedades reológicas y funcionales del almidón de tres variedades de papa criolla. *Información Tecnológica*, 30: 35-44. doi: 10.4067/S0718-07642019000600035
- Šoltýs, A., Hronský, V., Šmídová, N., Olčák, D., Ivanič, F., and Chodák, I. 2019. Solid-state <sup>1</sup>H and <sup>13</sup>C NMR of corn starch plasticized with glycerol and urea. *European Polymer Journal*. 117: 19-27. doi: 10.1016/j.eurpolymj.2019.04.042
- Soto, D., and Oliva, H. 2012. Métodos para preparar hidrogeles químicos y físicos basados en almidón: Una revisión. *Revista Latinoamericana de Metalurgia y Materiales* 32: 154-175.
- Thakur, M., Rai, A.K., Mishra, B.B., and Singh, S.P. 2021. Novel insight into valorization of potato peel biomass into type III resistant starch and maltooligosaccharide molecules. *Environmental Technology & Innovation*. 24: 101827. doi: 10.1016/j.eti.2021.101827

- Thérien-Aubin, H., Janvier, F., Baille, W.E., Zhu, X.X., and Marchessault, R. H. 2007. Study of hydration of cross-linked high amylose starch by solid state <sup>13</sup>C NMR spectroscopy. *Carbohydrate Research*. 342: 1525-1529. doi: 10.1016/j.carres.2007.04.014
- Too, B. C., Van, N., and Thuy, N. M. 2022. Formulation and quality evaluation of noodles with starchy flours containing high levels of resistant starch. *Acta Scientiarum Polonorum Technologia Alimentaria*. 21: 145-154. doi: 10.17306/J.AFS.2022.1011
- Torres, B.M., Carmona, G.R., and Aguirre, C.A. 2015. Obtención y caracterización estructural y funcional de almidón acetilado de malanga (*Colocasia esculenta* Schott). *Revista Mexicana de Ciencias Agrícolas*. 6: 905-912.
- Torres, M. D., Fradinho, P., Rodríguez, P., Falqué, E., Santos, V., and Domínguez, H. 2020. Biorefinery concept for discarded potatoes: Recovery of starch and bioactive compounds. *Journal of Food Engineering*. 275: 109886. doi: 10.1016/j.jfoodeng.2019.109886
- Valle, C.M., García, C.J., Laos, A. Doris., Yarasca, C. E., Loyola, G.E., and Surco-Laos, F. 2019. Análisis proximal y cuantificación de antocianinas totales en *Zea mays* variedad morada sometido a diferentes procesos de secado. *Revista de la Sociedad Química del Perú*. 85: 109-115.
- Vargas, G., Martínez, P., and Velezmore, C. 2016. Propiedades funcionales de almidón de papa (*Solanum tuberosum*) y su modificación química por acetilación. *Scientia Agropecuaria*. 7: 223-230. doi: 10.17268/sci.agropecu.2016.03.09
- Verma, R., Jan, S., Rani, S., Jan, K., Swer, T.L., Prakash, K.S., Dar, M.Z., and Bashir, K. 2018. Physicochemical and functional properties of gamma irradiated buckwheat and potato starch. *Radiation Physics and Chemistry*. 144: 37-42. doi: 10.1016/j.radphyschem.2017.11.009
- Yadav, U., Singh, N., Arora, S., and Arora, B. 2019. Physicochemical, pasting, and thermal properties of starches isolated from different adzuki bean (*Vigna angularis*) cultivars. *Journal of Food Processing and Preservation*, 43: e14163. doi: 10.1111/jfpp.14163
- Zhang, H., He, F., Wang, T., and Chen, G. 2021. Thermal, pasting, and rheological properties of potato starch dual-treated with CaCl<sub>2</sub> and dry heat. *LWT*. 146: 111467. doi: 10.1016/j.lwt.2021.111467
- Zhou, G., Luo, Z., and Fu, X. 2014. Preparation and characterization of starch nanoparticles in ionic liquid-in-oil microemulsions system. *Industrial Crops and Products*. 52: 105-110. doi: 10.1016/j.indcrop.2013.10.019